U2R: UNDERWATER ULTRASONIC REFLECTION WAVE DATASET TOWARD POSE-INVARIANT MATERIAL RECOGNITION

Mayuka Kono[⋆], *Yutaro Hirao*[⋆], *Monica Perusquía-Hernández*[⋆], *Naoya Isoyama*[†], *Hideaki Uchiyama*[⋆], *Nobuchika Sakata*[‡], *Jun Takamatsu*[§], *and Kiyoshi Kiyokawa*[⋆]

[⋆] Graduate School of Science and Technology, Nara Institute of Science and Technology, Japan
[†] Faculty of Social Information Studies, Otsuma Women's University, Japan
[‡] Faculty of Advanced Science and Technology, Ryukoku University, Japan
[§] Applied Robotics Research, Microsoft USA, USA

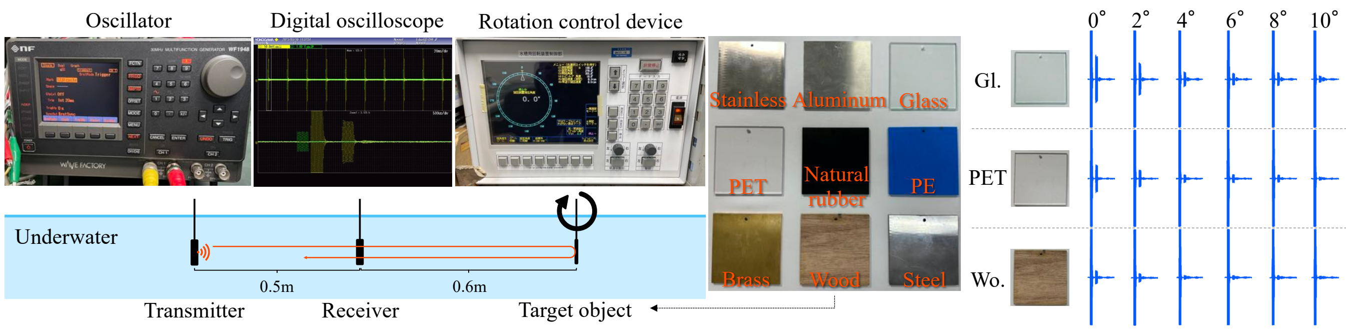

Fig. 1. Overview of our dataset.

ABSTRACT

In underwater environments, the reflected ultrasonic waves from objects generally provide more than just information about their color and shape for object recognition. Previous studies have overlooked the influence of object pose on these wave components. It is crucial to investigate how these poses affect the reflected wave components because object poses can vary widely and are often unpredictable in real-world scenarios. In this work, we introduce a novel dataset comprising reflected wave components collected from objects made of various materials and observed from various angles. We also show the preliminary evaluations on the performance of machine learning-based material classification on object pose. Our results indicate that the accuracy is consistently high ($\geq 91\%$) for known angles but significantly drops ($< 60\%$) when dealing with unknown angles in most cases. Based on these evaluations, we suggest several directions for future research. Our dataset is available at `https://github.com/Nyamotaro/U2R`.

***Index Terms*—** material recognition, underwater acoustics, ultrasonics, acoustic sensing, robotics

1. INTRODUCTION

Understanding underwater conditions in oceans, rivers, and lakes is crucial for ensuring the safety of vessel navigation and the integrity of structures like submarine oil pipelines [1, 2]. It also plays a vital role in protecting the underwater environment. Recently, there has been a growing focus on research aimed at addressing environmental concerns [3, 4, 5, 6, 7, 8]. Some of these studies leverage underwater robotic technologies to investigate aquatic waste, which is a significant societal issue [4, 5, 6, 9].

Previous studies on underwater object recognition have primarily relied on camera images [10, 11, 12, 13, 14, 15]. However, they generally encountered limitations. RGB-D cameras are hindered by turbidity and light variations while effectively capturing scene details [16]. Additionally, identifying materials based solely on color and shape can be challenging [17, 18]. In contrast, some methods have utilized acoustic cameras, offering advantages such as reduced sensitivity to turbidity and light intensity [12, 19]. However, they still face difficulties in material recognition because they depend on shape characteristics [20]. It is worth noting that the underwater environment is highly variable, with turbidity and light intensity fluctuating depending on the location. Furthermore, underwater waste can encompass transparent objects with similar shapes but made from different materials, such as plastic and glass products. These are important but difficult challenges to be solved. Using one-dimensional data from reflected wave components during ultrasonic irradiation allows us to go beyond color and shape. Sphere material classification has been demonstrated using wave components in machine learning models [21, 22].

Datasets are essential for achieving machine learning-based underwater material recognition using one-dimensional information on reflected wave components. There are still some limitations, although undisclosed datasets collected exist [21, 22, 23]. First, the number of material types is small. In practice, more various materials exist in the real-world underwater environment. Second, the data is only collected from spheres. The effect of object pose on reflected waves can be ignored by targeting a sphere. However, the object's shape is varied and unknown in the real environment.

This paper proposes a novel dataset with reflected wave data from flat plates constructed from nine different materials. This dataset encompasses data gathered at four distinct frequencies un-

Table 1. Comparison to existing datasets.

Dataset	Pub.	UW	Obj.	Mat.	Ang.	Freq.
Kang [25]	✗	✗	Plate	9	✗	MUX
Qing [21]	✗	✓	Sphere	3	✗	MUX
Dmitrieva [23]	✗	✓	Sphere	4	✗	MUX
Our dataset	✓	✓	Plate	9	✓	Single

der six varying angular conditions. We also show the preliminary evaluations on machine learning-based material classification performance using AutoGluon [24]. Based on these evaluations, we suggest several directions for future research. Our primary contributions are summarized as follows:

- We provide the world-first underwater reflected wave dataset resulting from ultrasonic irradiation at multiple frequencies and incident angles.
- The experiments demonstrate that the object's pose significantly impacts the material classification accuracy.
- We discuss important research topics contributing to underwater material recognition.

2. RELATED WORK

Table 1 compares our dataset with previous datasets. We introduce the details and the differences with ours.

Kang et al. conducted research collecting reflected wave components by exposing aerial objects to broadband ultrasonic waves generated based on bat echolocation sounds [25]. Their dataset consists of measurements taken from the object's front at 12 different distances and includes nine distinct materials, such as a blanket and an iron plate. However, this dataset lacks information on reflected waves corresponding to different object poses.

Qing et al. focused their efforts on gathering reflected wave components from underwater objects exposed to three distinct broadband pulse waves, ranging from 40 to 80 kHz, generated based on dolphin clicks [21]. Their dataset comprises frontal measurements conducted at a fixed distance for aluminum, brass, and stainless steel. Notably, their dataset exclusively pertains to spheres, where the effect of object pose is negligible, and does not encompass reflected wave data for varying object poses.

Dmitrieva et al. collected reflected wave components from underwater objects using broadband pulsed waves spanning 52 to 136 kHz [22, 23]. Their dataset includes data for aluminum, stainless steel, brass, and copper, acquired from the object's front at distances ranging from 1 to 3 m. Similar to [21] dataset, they focused on spheres with a two-layer structure and did not incorporate reflected wave data for diverse object poses. It is worth highlighting that all these mentioned datasets are currently undisclosed.

Our dataset uniquely captures reflected wave components for various object poses achieved by adjusting the angle of flat plates submerged in water. We targeted nine different materials and gathered reflected wave components by irradiating objects with four distinct single-frequency ultrasound waves. Importantly, our dataset is intended for public release upon publication, promoting transparency and collaboration within the research community.

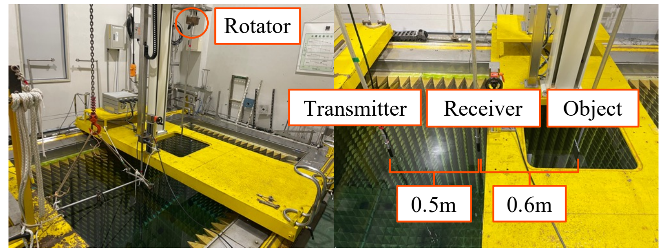

Fig. 2. Measurement environment.

3. DATA COLLECTION

3.1. Overview

Our dataset comprises reflected wave data obtained at four distinct frequencies and six different angular conditions, covering nine materials. Each condition includes data from ten separate trials. A total of 2,160 waveform data are included in the dataset. Data collection followed specific parameters, including a 625 kHz sampling rate, a 0.2 kHz high-pass filter (HPF), and a 200 kHz low-pass filter (LPF). In the following subsections, we will detail our data collection methodology.

3.2. Theoretical principles to be considered

Distance between the transmitter/receiver and the target object. When measuring reflected wave signals, accounting for the distance between the transmitter/receiver and the object is crucial, especially in the near-field region. The near-field represents an area where the wave phases are intricate, and the sound pressure distribution near the transducer is complex [26]. Various equations have been defined for calculating the near-field region [27]. We use the following equation to calculate the distance of the near-field in this work:

$$L_{near} = \frac{D^2}{\lambda} \tag{1}$$

where L_{near} represents the distance of the near-field (m), D stands for the diameter of the transmitter's aperture or the width of the square plate (m), and λ corresponds to the wavelength (m). In our work, we primarily focus on the near-field region from the target object to the receiver, as the near-field region from the transmitter is negligible. This equation allows us to determine the distance between the transmitter and receiver concerning the target object.

Signal transmission and reception. Our transmit signal is a sinusoidal waveform generated by an oscillator with a precisely chosen pulse length of 0.3 ms and a 20 ms transmission interval. The 0.3 ms pulse length ensures an integer number of cycles for each frequency condition, serving our purposes optimally, while the 20ms interval eliminates multipath effects. The transmitted signal for each frequency condition includes 15 cycles for 50 kHz, 18 cycles for 60 kHz, 21 cycles for 70 kHz, and 24 cycles for 80 kHz. Received signals fall into two categories: direct wave and reflected wave signals. Both are captured using a digital oscilloscope with a 625 kHz sampling rate. To ensure data reliability, we apply filtering techniques, including a 0.2 kHz high-pass filter (HPF) and a 200 kHz low-pass filter (LPF). These filter settings have been rigorously validated for effective noise removal.

3.3. Method

Devices. The measurement system in Figure 1 (left), consists of key components: two underwater transducers (OST 2150, OKI Com-Echoes), an oscillator (WF1948, NF), a power amplifier (HSA4011, NF), a fixed attenuator (40 dB attenuation), a preamplifier (5307, NF), a digital oscilloscope (DLM2054, YOKOGAWA), and a filter. One transducer serves as the transmitter, and the other as the receiver. The oscillator signal is amplified 20 times by a power amplifier, then further amplified 10 times through a preamplifier with a fixed attenuator before reaching the digital oscilloscope. The received signal goes through a 20x preamplification and is processed with a HPF at 0.2 kHz and a LPF at 200 kHz via a dedicated filter module before being fed into the digital oscilloscope.

Environment. The measurements were conducted in an anechoic tank at OKI Com-Echoes Co., Ltd. in Numazu City, Shizuoka, Japan. The tank measured 5.0 m (L) $\times$ 2.5 m (W) $\times$ 3. m (H) and used tap water at 14.6°C as the medium. To ensure optimal conditions, we set the receiver-to-object distance at 0.6 m using Equation (1) and the transmitter-to-receiver distance at 0.5 m. This resulted in a 1.1 m distance between the transmitter and the target object. This distance was chosen to minimize noise from the tank's dimensions. All three components (transmitter, receiver, and target object) were positioned 1.2 m below the water surface using a dedicated jig. The target object was mounted on a device that allowed precise rotation in 0.1° increments, ensuring precise control during experiments.

Conditions. The measurement conditions are summarized in Table 2. We used stainless steel, aluminum, glass, PET, natural rubber, PE foam, brass, wood, and steel in Figure 1 (center). Each object was a flat plate measuring 100 mm (L) $\times$ 100 mm (W) $\times$ 5.0 mm (thickness), except for wood, which was 5.5 mm thick. To ensure secure attachment to the jig, we added holes at the top edge of all objects and at the lower end, where weights were attached for natural rubber and PE due to buoyancy issues. We explored four ultrasonic frequency settings: 50 kHz, 60 kHz, 70 kHz, and 80 kHz. Additionally, we investigated six different incident angles for ultrasonic waves on the object surface: 0°, 2°, 4°, 6°, 8°, and 10°. This resulted in a total of 216 conditions, combining nine materials, four frequencies, and six angles. Each of these 216 conditions was tested in 10 separate trials, ensuring the collection of comprehensive and reliable data.

Procedure. The data collection process adhered to the following procedure:

1. All objects were immersed in the same water as the measurement environment overnight.

2. The measurements were conducted in the following order: stainless, aluminum, glass, PET, natural rubber, PE, brass, wood, and steel. For each material, the measurements were performed 10 times at each of the following conditions:

    - Incident Angles: 0, 2, 4, 6, 8, and 10 ($^\circ$).

    - Ultrasonic Frequencies: 50, 60, 70, and 80 (kHz).

Step 1 was undertaken because it was observed that when objects were placed in water without this treatment, a layer of air could form on the object's surface. This air layer had a discernible impact on the measurement data, highlighting the necessity of ensuring consistent and accurate experimental conditions.

Table 2. Measurement conditions.

Mat.	Freq. (kHz)	Ang. ($^\circ$)
Stainless	50, 60, 70, 80	0, 2, 4, 6, 8, 10
Aluminum	50, 60, 70, 80	0, 2, 4, 6, 8, 10
Glass	50, 60, 70, 80	0, 2, 4, 6, 8, 10
PET	50, 60, 70, 80	0, 2, 4, 6, 8, 10
Natural rubber	50, 60, 70, 80	0, 2, 4, 6, 8, 10
PE	50, 60, 70, 80	0, 2, 4, 6, 8, 10
Brass	50, 60, 70, 80	0, 2, 4, 6, 8, 10
Wood	50, 60, 70, 80	0, 2, 4, 6, 8, 10
Steel	50, 60, 70, 80	0, 2, 4, 6, 8, 10

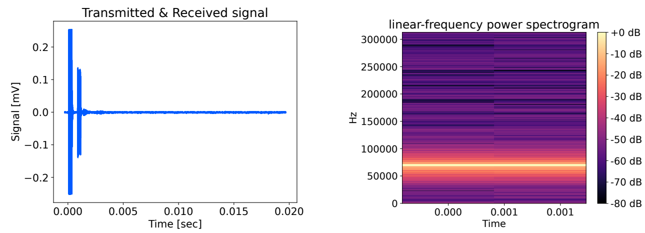

(a) Received wave. (b) Spectrogram.

Fig. 3. Stainless, 70 kHz and 0° condition.

4. MATERIAL CLASSIFICATION

4.1. Feature extraction

Figure 3(a) shows an example of the received signal waveform for one trial, taken at 70 kHz and 0° for the stainless material. Subsequently, cross-correlation values were computed between the transmitted and received signals, which facilitated the determination of the required reflected wave component of the received signal. For this analysis, it was found that the number of samples required was 231. However, to meet the condition necessary for the subsequent Fourier transform, which mandates a power-of-two sample size, 256 samples were employed to extract the reflected wave components. The Short-Time Fourier Transform (STFT) was then applied to these extracted reflected wave components, with a Hann window chosen as the window function. A window size of 1024 was utilized. The outcome of this process was a spectrogram, where frequency and time were represented on the vertical and horizontal axes, respectively, and dB values were denoted by the color density. Figure 3(b) illustrates a spectrogram for stainless material at 70 kHz and 0°. The dB values extracted from the spectrogram served as high-dimensional feature vectors for further analysis.

4.2. Results

The classification accuracy was evaluated after features were labeled with material types to evaluate the effect of the angle on the accuracy. AutoGluon [24] was employed as the evaluation tool, as detailed in the study. The feature vectors obtained from the spectrogram data were labeled with their corresponding material types. It is noteworthy that in this analysis, only models with a runtime of 120 s or less were utilized. This runtime constraint was imposed to ensure the efficiency of the model evaluation process while maintaining reasonable computational demands.

Same angle conditions. The test conducted aimed to establish the criteria for evaluating the impact of the angle on classification accu-

Table 3. Classification results in the same angle conditions.

Freq.	Ang.					
	0°	2°	4°	6°	8°	10°
50 kHz	1.0	0.89	0.93	0.89	0.93	1.0
60 kHz	1.0	1.0	1.0	1.0	1.0	1.0
70 kHz	1.0	1.0	0.89	1.0	1.0	0.93
80 kHz	1.0	1.0	0.96	1.0	1.0	0.96

Table 4. Classification results in the mixed angle conditions.

Freq.	Acc.
50 kHz	0.92
60 kHz	0.96
70 kHz	0.94
80 kHz	0.91

racy. In this test, the data was split into training and test sets with a ratio of 7:3. The split was executed in a manner that ensured the proportion of each material label was consistent between the training and test data sets. The results of this evaluation, as presented in Table 3, indicate that in the majority of cases, an accuracy of 100% was attained. This suggests that the classification model performed exceptionally well in correctly classifying the materials, reflecting the high quality and reliability of the dataset and the effectiveness of the classification process.

Mixed angle conditions. This test aimed to verify the classification accuracy when using training data that encompassed all angular conditions. Similar to the previous test, the data was divided into training and test sets in a 7:3 ratio, ensuring that the proportion of each material label was consistent between the two sets. The outcomes, as illustrated in Table 4, reveal that for all frequency conditions, the classification model achieved an accuracy of 91% or greater. These results indicate that data associated with trained angles could be effectively discriminated with a high degree of accuracy. This underscores the robustness of the classification model, especially when the model is well-trained across various angular conditions.

Unknown angle conditions (Blind test). This test assessed classification accuracy for data with unknown angular conditions. Training data included five out of six angular conditions, while the unseen test data represented the remaining condition. Results in Table 5 mostly showed accuracy below 60%, with a minimum of 11%. The model struggled to classify materials accurately in unknown angular conditions, often misclassifying them even within the same material category. This highlights a significant challenge, underscoring the need for further investigation in handling such scenarios.

4.3. Discussion

Firstly, the variances observed in the results under the same angle conditions can be attributed to factors such as frequency-related sensor characteristics and non-linear underwater wave phenomena. Reflected waves exhibit nonlinearity due to components like specular and scattered reflections. Our research aims to model these phenomena using physics-based machine learning techniques. Addressing this challenge is a key objective for future work.

Secondly, high accuracy in classifying objects was achieved under mixed angle conditions, demonstrating the model's effectiveness in familiar scenarios. However, a substantial drop in accuracy occurred when dealing with unknown angles, highlighting the challenge posed by varying reflected wave components based on the object's pose.

Table 5. Classification results in the unknown angle conditions.

Freq.	Unknown Ang.					
	0°	2°	4°	6°	8°	10°
50 kHz	0.70	0.80	0.53	0.38	0.29	0.29
60 kHz	0.58	0.67	0.48	0.33	0.34	0.13
70 kHz	0.42	0.61	0.20	0.22	0.41	0.22
80 kHz	0.33	0.56	0.23	0.27	0.24	0.11

Accurate material classification heavily depends on having pose-specific reflected wave data. Real-world environments present diverse and unknown object poses, necessitating the development of accurate material recognition methods. We primarily focused on using amplitude information from single-frequency ultrasonic waves in this study. Notably, reflected wave components contain phase differences in addition to amplitude. We suggest that combining and analyzing data collected under multiple frequency conditions can provide valuable insights. These insights may help address challenges related to object poses by leveraging domain knowledge about angles and reflected wave components, offering a promising avenue for future research.

Moreover, many studies have been tackling the challenge of poor image quality underwater in image-based methods that capture scene details like object positions [28, 29, 30]. In the future, we hope that high-performance underwater material recognition methods will be achieved by combining these advanced image-based techniques with our research insight.

5. CONCLUSION

We introduced a novel dataset containing one-dimensional reflected wave component data obtained by directing ultrasonic waves at different incident angles toward underwater objects. The material classification evaluation demonstrates high accuracy when the model is trained on specific angles. However, accuracy drops significantly when dealing with unknown angles, emphasizing the challenge posed by object pose variations on reflected wave components.

The impact of object pose on reflected wave components is a substantial challenge, especially in real-world scenarios with diverse and unpredictable object orientations. The study suggests that feature extraction from data collected under different frequency conditions can provide not only amplitude information but also valuable insights like phase differences. Leveraging this broader information as domain knowledge holds promise for addressing object-pose-related issues and advancing the development of robust and accurate material recognition methods. This research paves the way for exciting possibilities in future studies within this field.

6. ACKNOWLEDGEMENT

This work was supported by JST, the establishment of university fellowships towards the creation of science technology innovation, Grant Number JPMJFS2137.

7. REFERENCES

[1] Swagat Chutia, Nayan M Kakoty, and Dhanapati Deka, "A review of underwater robotics, navigation, sensing techniques and applications," *Advances in Robotics*, pp. 1–6, 2017.

- [2] Kai Sun, Weicheng Cui, and Chi Chen, "Review of underwater sensing technologies and applications," *Sensors*, vol. 21, no. 23, pp. 7849, 2021.
- [3] Md Moniruzzaman, Syed Mohammed Shamsul Islam, Mohammed Bennamoun, and Paul Lavery, "Deep learning on underwater marine object detection: A survey," in *18th International Conference on Advanced Concepts for Intelligent Vision Systems*, 2017, pp. 150–160.
- [4] Michael Fulton, Jungseok Hong, Md Jahidul Islam, and Junaed Sattar, "Robotic detection of marine litter using deep visual detection models," in *International Conference on Robotics and Automation*, 2019, pp. 5752–5758.
- [5] Jun-Ichiro Watanabe, Yang Shao, and Naoto Miura, "Underwater and airborne monitoring of marine ecosystems and debris," *Journal of Applied Remote Sensing*, vol. 13, no. 4, pp. 044509, 2019.
- [6] Ivana Marin, Saša Mladenović, Sven Gotovac, and Goran Zaharija, "Deep-feature-based approach to marine debris classification," *Applied Sciences*, vol. 11, no. 12, pp. 5644, 2021.
- [7] Naoki Shirakura, Takuya Kiyokawa, Hikaru Kumamoto, Jun Takamatsu, and Tsukasa Ogasawara, "Collection of marine debris by jointly using uav-uuv with gui for simple operation," *IEEE Access*, vol. 9, pp. 67432–67443, 2021.
- [8] Yuwei Cheng, Jiannan Zhu, Mengxin Jiang, Jie Fu, Changsong Pang, Peidong Wang, Kris Sankaran, Olawale Onabola, Yimin Liu, Dianbo Liu, et al., "Flow: A dataset and benchmark for floating waste detection in inland waters," in *IEEE/CVF International Conference on Computer Vision*, 2021, pp. 10953–10962.
- [9] Matias Valdenegro-Toro, "Deep neural networks for marine debris detection in sonar images," *arXiv preprint arXiv:1905.05241*, 2019.
- [10] Sejin Lee, Byungjae Park, and Ayoung Kim, "Deep learning from shallow dives: Sonar image generation and training for underwater object detection," *arXiv preprint arXiv:1810.07990*, 2018.
- [11] Dario Lodi Rizzini, Fabjan Kallasi, Fabio Oleari, and Stefano Caselli, "Investigation of vision-based underwater object detection with multiple datasets," *International Journal of Advanced Robotic Systems*, vol. 12, no. 6, pp. 77, 2015.
- [12] Matheus dos Santos, Paulo Drews, Pedro Núñez, and Silvia Botelho, "Object recognition and semantic mapping for underwater vehicles using sonar data," *Journal of Intelligent & Robotic Systems*, vol. 91, pp. 279–289, 2018.
- [13] Fenglei Han, Jingzheng Yao, Haitao Zhu, Chunhui Wang, et al., "Underwater image processing and object detection based on deep cnn method," *Journal of Sensors*, vol. 2020, 2020.
- [14] Divas Karimanzira, Helge Renkewitz, David Shea, and Jan Albiez, "Object detection in sonar images," *Electronics*, vol. 9, no. 7, pp. 1180, 2020.
- [15] Yongcan Yu, Jianhu Zhao, Quanhua Gong, Chao Huang, Gen Zheng, and Jinye Ma, "Real-time underwater maritime object detection in side-scan sonar images based on transformer-yolov5," *Remote Sensing*, vol. 13, no. 18, pp. 3555, 2021.
- [16] Cameron Fabbri, Md Jahidul Islam, and Junaed Sattar, "Enhancing underwater imagery using generative adversarial networks," in *IEEE International Conference on Robotics and Automation*, 2018, pp. 7159–7165.
- [17] Philip Saponaro, Scott Sorensen, Abhishek Kolagunda, and Chandra Kambhamettu, "Material classification with thermal imagery," in *IEEE Conference on Computer Vision and Pattern Recognition*, 2015, pp. 4649–4656.
- [18] Kenichiro Tanaka, Yasuhiro Mukaigawa, Takuya Funatomi, Hiroyuki Kubo, Yasuyuki Matsushita, and Yasushi Yagi, "Material classification using frequency-and depth-dependent time-of-flight distortion," in *IEEE Conference on Computer Vision and Pattern Recognition*, 2017, pp. 79–88.
- [19] Mateusz Ochal, Jose Vazquez, Yvan Petillot, and Sen Wang, "A comparison of few-shot learning methods for underwater optical and sonar image classification," in *Global Oceans*, 2020, pp. 1–10.
- [20] Deepak Singh and Matias Valdenegro-Toro, "The marine debris dataset for forward-looking sonar semantic segmentation," in *IEEE/CVF International Conference on Computer Vision*, 2021, pp. 3741–3749.
- [21] Xin Qing, Donghu Nie, Gang Qiao, and Jiansheng Tang, "Classification for underwater small targets with different materials using bio-inspired dolphin click," in *IEEE/OES China Ocean Acoustics*, 2016, pp. 1–6.
- [22] Mariia Dmitrieva et al., *Object characterisation using wideband sonar pulses*, Ph.D. thesis, Heriot-Watt University, 2018.
- [23] Mariia Dmitrieva, Keith Brown, Gary Heald, and David Lane, "Material recognition based on the time delay of secondary reflections using wideband sonar pulses," *IET Radar, Sonar & Navigation*, vol. 13, no. 11, pp. 2034–2040, 2019.
- [24] Nick Erickson, Jonas Mueller, Alexander Shirkov, Hang Zhang, Pedro Larroy, Mu Li, and Alexander Smola, "Autogluon-tabular: Robust and accurate automl for structured data," *arXiv preprint arXiv:2003.06505*, 2020.
- [25] Geon Kang and Seung-Chan Kim, "Deepecho: Echoacoustic recognition of materials using returning echoes with deep neural networks," *IEEE Transactions on Emerging Topics in Computing*, vol. 10, no. 1, pp. 450–462, 2020.
- [26] A Lukosevicius and R Jurkonis, "Ultrasonic near field in lossy media: Method of simulation," *Ultragarsas/Ultrasound*, vol. 27, no. 1, pp. 33–37, 1997.
- [27] Kenneth G Foote, "Discriminating between the nearfield and the farfield of acoustic transducers," *The Journal of the Acoustical Society of America*, vol. 136, no. 4, pp. 1511–1517, 2014.
- [28] Wei-Hong Lin, Jia-Xing Zhong, Shan Liu, Thomas Li, and Ge Li, "Roimix: Proposal-fusion among multiple images for underwater object detection," in *IEEE International Conference on Acoustics, Speech and Signal Processing*, 2020, pp. 2588–2592.
- [29] Zhenqi Fu, Xiaopeng Lin, Wu Wang, Yue Huang, and Xinghao Ding, "Underwater image enhancement via learning water type desensitized representations," in *IEEE International Conference on Acoustics, Speech and Signal Processing*, 2022, pp. 2764–2768.
- [30] Ziyin Ma and Changjae Oh, "A wavelet-based dual-stream network for underwater image enhancement," in *IEEE International Conference on Acoustics, Speech and Signal Processing*, 2022, pp. 2769–2773.